PCCP

COMMUNICATION

View Article Online
View Journal | View Issue

Cite this: *Phys. Chem. Chem. Phys.*, 2015, **17**, 19690

Received 2nd June 2015,
Accepted 6th July 2015

DOI: 10.1039/c5cp03178h

www.rsc.org/pccp

Endohedral C_3 $Ca@B_{39}^+$ and C_2 $Ca@B_{39}^+$: axially chiral metalloborospherenes based on B_{39}^-†

Qiang Chen,[ab] Ting Gao,[a] Wen-Juan Tian,[a] Hui Bai,[a] Su-Yan Zhang,[a] Hai-Ru Li,[a] Chang-Qing Miao,[b] Yue-Wen Mu,[a] Hai-Gang Lu,*[a] Hua-Jin Zhai*[ac] and Si-Dian Li*[a]

Using the newly discovered borospherenes C_3 B_{39}^- and C_2 B_{39}^- as molecular devices and based on extensive global-minimum searches and first-principles calculations, we present herein the possibility of the first axially chiral metalloborospherenes C_3 $Ca@B_{39}^+$ (1, ^1A) and C_2 $Ca@B_{39}^+$ (2, ^1A), which are the global minimum and the second lowest-lying isomer of CaB_{39}^+, respectively. These metalloborospherene species turn out to be charge-transfer complexes $Ca^{2+}@B_{39}^-$ in nature, with the Ca centre on the C_3 or C_2 molecular axis donating one electron to the B_{39} cage which behaves like a superhalogen. Molecular orbital analyses indicate that C_3/C_2 $Ca^{2+}@B_{39}^-$ possess the universal bonding pattern of σ plus π double delocalization, similar to their C_3/C_2 B_{39}^- parents. Molecular dynamics simulations show that both C_3 $Ca@B_{39}^+$ (1) and C_2 $Ca@B_{39}^+$ (2) are dynamically stable at 200 K, with the former starting to fluctuate structurally at 300 K and the latter at 400 K, again similar to C_3/C_2 B_{39}^-. The infrared and Raman spectra of C_3/C_2 $Ca@B_{39}^+$ (1/2) are simulated and compared with those of C_3/C_2 B_{39}^- to facilitate their forthcoming experimental characterization.

The first endohedral metallofullerene, $La@C_{60}$, was discovered immediately after the discovery of C_{60} in 1985.[1] Various endohedral metallofullerenes and non-metal-doped fullerenes were subsequently synthesized and isolated,[1–9] including C_{5v} $Ca@C_{60}$ with a calcium atom inside C_{60} and $M@C_{76}$ (M = Ca, Sr, Sm, Yb) with an alkaline earth or rare earth metal inside chiral C_{76},[10] which remarkably enrich the chemistry of carbon fullerenes. Boron, the lighter neighbor of carbon in the periodic table, is characterized with multicenter chemical bonding, which compensates for boron's electron deficiency in solids and polyhedral molecules. Small boron clusters $B_n^{-/0}$ have proven to be planar or quasi-planar in a wide range of sizes (n = 3–25, 30, 35, 36) in a series of combined experimental and theoretical investigations.[11–19] The possibility of all-boron fullerenes was not considered before the celebrated I_h B_{80} buckyball was proposed in 2007,[20] which was built based on the C_{60} motif by capping all the twenty surface hexagons. However, B_{80} was later found to favor the core-shell-type structures at various theoretical levels.[21,22] Cage-like D_{2d} $B_{40}^{-/0}$, the first all-boron fullerenes referred to as borospherenes in literature, were discovered in 2014 in a combined experimental and theoretical investigation, revealing the planar-to-cage-like structural transition in $B_n^{-/0}$ at around $n \approx 40$.[23] The first axially chiral borospherenes C_3 B_{39}^- and C_2 B_{39}^-, the global minimum and the second lowest-lying isomer of B_{39}^-, respectively, were observed in 2015.[24] Two cationic chiral members C_1 B_{41}^+ and C_2 B_{42}^{2+} were recently presented to the borospherene family based on extensive global-minimum searches and first-principles calculations.[25] These borospherenes are all composed of twelve interwoven boron double-chains with six hexagonal/heptagonal faces and possess the universal bonding pattern of σ plus π double delocalization. B_{39}^-, B_{40}, B_{41}^+, and B_{42}^{2+} thus form a π-isovalent B_n^q series in different charge states ($q = n - 40$), which all have 12 multicenter two-electron π-bonds (12 mc-2e π) over a σ-skeleton made of n + 8 delocalized three-center two-electron σ-bonds (n + 8 3c-2e σ). The observation of the D_{2d} $B_{40}^{-/0}$ borospherenes leads to a quick surge of borospherene chemistry. The endohedral $M@B_{40}$ metalloborospherenes (M = Ca, Sr) were predicted to be viable species in a recent communication at the density functional theory (DFT) level.[26] A theoretical study on the electronic structure and electronic spectra of D_{2d} B_{40},[27] a topological analysis of D_{2d} B_{40},[28] and a computational investigation on the endohedral $M@B_{40}$ (M = Sc, Y, La)[29] quickly followed.

Using the C_3/C_2 B_{39}^- borospherenes as molecular devices and based on extensive first-principles calculations, we present herein the viability of the first axially chiral metalloborospherenes C_3 $Ca@B_{39}^+$ (**1**, ^1A) and C_2 $Ca@B_{39}^+$ (**2**, ^1A), which are the global minimum (GM) and the second lowest-lying isomer of CaB_{39}^+, respectively. These endohedral metalloborospherenes, along with

[a] *Nanocluster Laboratory, Institute of Molecular Science, Shanxi University, Taiyuan 030006, China. E-mail: luhg@sxu.edu.cn, hj.zhai@sxu.edu.cn, lisidian@sxu.edu.cn*

[b] *Institute of Materials Science and Department of Chemistry, Xinzhou Teachers' University, Xinzhou 034000, China*

[c] *State Key Laboratory of Quantum Optics and Quantum Optics Devices, Shanxi University, Taiyuan 030006, China*

† Electronic supplementary information (ESI) available. See DOI: 10.1039/c5cp03178h

their degenerate enantiomers, turn out to be charge-transfer complexes $Ca^{2+}@B_{39}^{-}$ in nature, in which the Ca centre donates one electron to the B_{39} cage. Both C_3 $Ca@B_{39}^{+}$ (**1**) and C_2 $Ca@B_{39}^{+}$ (**2**) are found to be dynamically stable at 200 K and structurally fluctuate above 400 K. Chemical bonding analyses indicate that these metalloborospherenes inherit the bonding pattern of σ plus π double delocalization from their C_3/C_2 B_{39}^{-} parents. These B_{39}^{-}-based metalloborospherenes differ from the previously reported $M@B_{40}$ (M = Ca, Sr)[26] in axial chirality. To facilitate their future spectral characterizations, the infrared (IR) and Raman spectra of C_3 $Ca@B_{39}^{+}$ (**1**) and C_2 $Ca@B_{39}^{+}$ (**2**) are predicted and compared with those of the C_3/C_2 B_{39}^{-} cages. Preliminary calculations indicate that, at the DFT-PBE0 level, the endohedral $Sr@B_{39}^{+}$ competes with its triple-ring tubular counterpart in thermodynamics, $Ca@B_{39}$ and $Sr@B_{39}$ are true minima of the neutrals, while $Be@B_{39}^{+}$ and $Mg@B_{39}^{+}$ appear to be less stable than their exohedral rivals due to size effect.[26]

The GM structural searches were performed for CaB_{39}^{+} using the Minima Hopping (MH) algorithm[30,31] at the DFT level. A total of 2328 stationary points were probed on the potential energy surface of the monocation, in combination with manual structural constructions based on the typical planar, cage-like, and tubular isomers of B_{39}^{-}.[24] Low-lying isomers were then fully optimized and their relative energies evaluated at both the hybrid DFT-PBE0[32] and CAM-B3LYP (which includes the long-range corrections using the Coulomb attenuating method)[33] levels with the 6-311+G(d) basis set[34] as implemented in the Gaussian 09 suite.[35] The relative stabilities of the five lowest-lying isomers were further refined using the more accurate coupled cluster method with triple excitations (CCSD(T))[36–38] implemented in MOLPRO[39] with the 6-31G(d) basis set at the PBE0 geometries. Molecular dynamics (MD) simulations were performed for the monocations at 200, 300, and 400 K for 30 ps using the software suite CP2K.[40] The optimized endohedral C_3/C_2 $Ca@B_{39}^{+}$ (**1**/**2**) and their degenerate enantiomers C_3/C_2 $Ca@B_{39}^{+}$ (**1′**/**2′**) are depicted in Fig. 1. More alternative isomers are summarized in Fig. S1 in the ESI.† Fig. 2 shows the molecular orbital energy levels of C_3/C_2 $Ca@B_{39}^{+}$ (**1**/**2**) at DFT-PBE0. The bonding patterns of C_3/C_2 $Ca@B_{39}^{+}$ (**1**/**2**) are analyzed in Fig. 3 using the adaptive natural density partitioning (AdNDP) method that includes multicenter two-electron (mc-2e) interactions.[41]

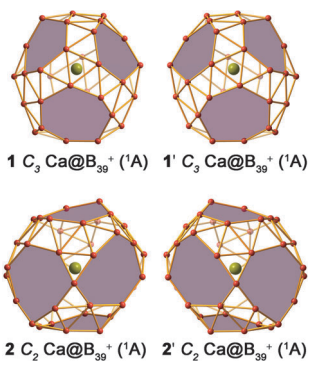

Fig. 1 Optimized structures of the axially chiral endohedral C_3 $Ca@B_{39}^{+}$ (**1**) and C_2 $Ca@B_{39}^{+}$ (**2**) and their degenerate enantiomers C_3 $Ca@B_{39}^{+}$ (**1′**) and C_2 $Ca@B_{39}^{+}$ (**2′**) at the PBE0/6-311+G(d) level.

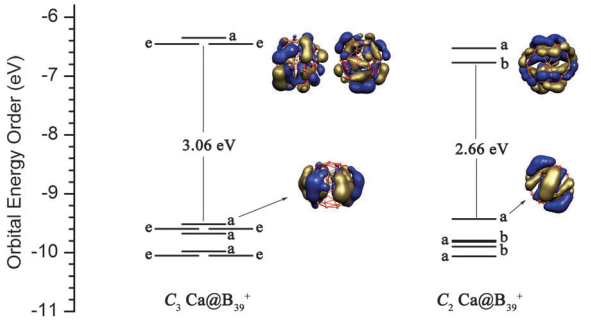

Fig. 2 Molecular orbital energy levels of C_3 $Ca@B_{39}^{+}$ (**1**, ^{1}A) and C_2 $Ca@B_{39}^{+}$ (**2**, ^{1}A) at the DFT-PBE0/6-311+G(d) level. The HOMO and LUMO pictures are depicted.

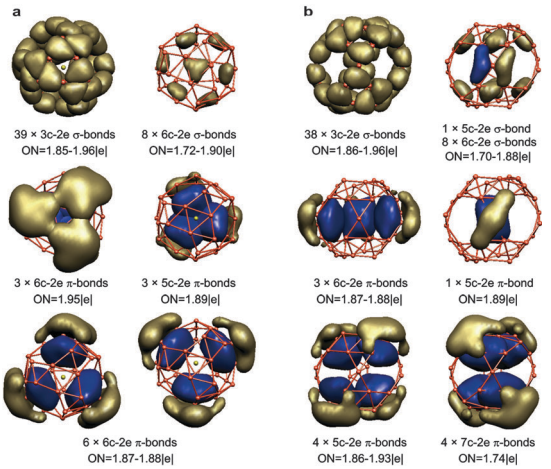

Fig. 3 AdNDP bonding patterns of C_3 $Ca@B_{39}^{+}$ (**1**) (a) and C_2 $Ca@B_{39}^{+}$ (**2**) (b). The occupation numbers (ONs) are indicated.

Fig. 4 shows the IR and Raman spectra of C_3 $Ca@B_{39}^{+}$ (**1**) and C_2 $Ca@B_{39}^{+}$ (**2**), as compared with those of C_3 B_{39}^{-} and C_2 B_{39}^{-}, respectively. We mainly focus on the DFT-PBE0 results in the following discussion, which are generally well supported by the CAM-B3LYP data (Fig. S1, ESI†).

Considering the fact that C_3 B_{39}^{-} and C_2 B_{39}^{-} borospherenes coexist in the gas phase,[24] we started our structural searches for CaB_{39}^{+} from the initial structures of C_3 $Ca@B_{39}^{+}$ and C_2 $Ca@B_{39}^{+}$ which were manually constructed by locating a Ca atom on the two- or three-fold molecular axis inside the B_{39}^{-} cage. Interestingly, both the C_3 B_{39}^{-} and C_2 B_{39}^{-} cages remain almost intact during the structural optimizations. More encouragingly, the optimized closed-shells C_3 $Ca@B_{39}^{+}$ (**1**, ^{1}A) and C_2 $Ca@B_{39}^{+}$ (**2**, ^{1}A) appear to be the global minimum and the second lowest-lying isomer of CaB_{39}^{+}, respectively, with the former being 0.26 and 0.15 eV more stable than the latter at the DFT-PBE0 and CAM-B3LYP levels. At the CCSD(T) level, C_3 $Ca@B_{39}^{+}$ (**1**) and C_2 $Ca@B_{39}^{+}$ (**2**) turn out to be almost isoenergetic with the minor relative energy of 0.03 eV, suggesting that the two close-lying isomers compete in thermodynamics and may coexist in experiments, similar to the situation of C_3/C_2 B_{39}^{-}.[24] The third and fourth lowest-lying C_1 $Ca@B_{39}^{+}$ (**3**) and C_1 $Ca@B_{39}^{+}$ (**4**), which are the positional isomers of C_2 $Ca@B_{39}^{+}$ (**2**) with two hexagons and four heptagons on the surface,

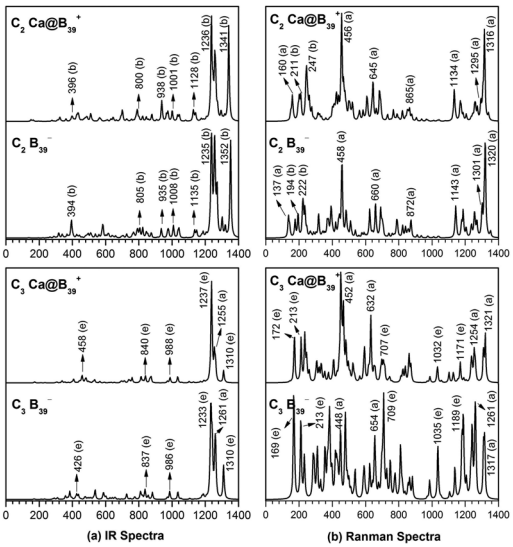

Fig. 4 Simulated IR (a) and Raman (b) spectra of C_3 Ca@B_{39}^+ (**1**) and C_2 Ca@B_{39}^+ (**2**) compared with those of their C_3 B_{39}^- and C_2 B_{39}^- parents.

lie 0.17 and 0.24 eV higher than C_3 Ca@B_{39}^+ (**1**) at CCSD(T), respectively. The fifth lowest-lying C_1 Ca@B_{39}^+ (**5**) with one pentagon, three hexagons, and three heptagons on the cage surface appears to be 0.45 eV higher than C_3 Ca@B_{39}^+ (**1**) at CCSD(T). The typical triple-ring tubular C_s CaB_{39}^+ (**6**) with a Ca on the top, the exohedral C_1 Ca&B_{39}^+ (**18**) with a η^7-Ca face-capping a heptagon on the surface, and the quasi-planar C_s CaB_{39}^+ (**30**) with a tri-coordinate Ca on one edge of the C_s B_{39}^- with a hexagon hole at the centre[24] turn out to be at least 0.60 eV less stable than C_3 Ca@B_{39}^+ (**1**) at DFT-PBE0 (Fig. S1, ESI†). The Ca atom effectively stabilizes the endohedral configurations (**1–5**), making them energetically favourable with respect to other low-lying isomers.

Vibrational analyses show that C_3 Ca@B_{39}^+ (**1**) possesses the smallest vibrational frequency of ν_{min} = 144 cm^{-1} (a mode), in which the Ca centre vibrates vertically along the three-fold molecular axis. In contrast, C_2 Ca@B_{39}^+ (**2**) has a small imaginary vibrational frequency of ν_{min} = 18i cm^{-1} (b mode), which leads to a slightly distorted C_1 Ca@B_{39}^+ with ν_{min} = 18 cm^{-1} (a mode) when fully optimized. However, with zero-point corrections, C_2 Ca@B_{39}^+ turns out to be isoenergetic with the distorted C_1 Ca@B_{39}^+. They correspond practically to the same structure with the Ca centre lying 3.03 and 3.09 Å from the tetracoordinate B at the "defect" site on the front and the boron double chain on the back in C_2 B_{39}^- (Fig. 1), respectively,[24] similar to the situation in C_{2v} Ca@B_{40}.[26] To the best of our knowledge, C_3/C_2 Ca@B_{39}^+ (**1/2**) are the first axially chiral metalloborospherenes reported to date, with the Ca centre lying exactly on the C_3 or C_2 molecular axis inside the B_{39} cage. The observed borospherenes D_{2d} B_{40} and C_2/C_3 B_{39}^- are about 1.0 Å smaller than C_{60} in diameters,[23,24] making them more suitable to host a metal atom inside on the two- or three-fold molecular axis.[26,28]

The high stabilities of these metalloborospherenes originate from their electronic structure and bonding patterns. Natural bonding orbital analyses show that the Ca centre in C_3 Ca@B_{39}^+ (**1**) and C_2 Ca@B_{39}^+ (**2**) carries a positive charge of +1.58 and +1.60 |e|, respectively, with the corresponding electronic configurations of Ca [Ar]$4s^{0.20}3d^{0.18}$ and Ca [Ar]$4s^{0.20}3d^{0.16}$. These results clearly indicate that the Ca centre in CaB_{39}^+ donates one electron to the B_{39} cage that behaves like a superhalogen.[42] The charge-transfer Ca^{2+}@B_{39}^- (**1/2**) complexes mainly show ionic interactions between the Ca^{2+} centre and the B_{39}^- cage. C_3/C_2 Ca@B_{39}^+ (**1/2**) may also benefit from the weak back-donations from the delocalized π orbitals of B_{39}^- to Ca 3d atomic orbitals (see below). As indicated in Fig. 2, C_3 Ca@B_{39}^+ (**1**) and C_2 Ca@B_{39}^+ (**2**) possess the huge HOMO–LUMO gaps of 3.06 and 2.66 eV at DFT-PBE0, respectively, well comparable with the values of 2.89, 2.73, and 3.13 eV obtained for C_3 B_{39}^-, C_2 B_{39}^-, and D_{2d} B_{40} at the same level,[23,24] The calculated formation energies of C_3 Ca@B_{39}^+ (**1**) and C_2 Ca@B_{39}^+ (**2**) are −119.6 and −113.0 kcal mol^{-1} at DFT-PBE0 with respect to Ca^+ + B_{39} = CaB_{39}^+ and −302.9 and −299.3 kcal mol^{-1} with respect to Ca^{2+} + B_{39}^- = CaB_{39}^+, respectively, further demonstrating the high thermodynamic stabilities of these monocation complexes.

AdNDP analyses unveil the bonding patterns of these $Ca^{2+}B_{39}^-$ complexes. As shown in Fig. 3a, C_3 Ca@B_{39}^+ (**1**) possesses 39 3c-2e σ and 8 6c-2e σ bonds. As the central B_3 triangles make major contribution to the 6c-2e σ bonds, these σ interactions can be practically treated as 47 3c-2e σ bonds evenly distributed on the cage surface with one 3c-2e σ bond on each B_3 triangle. Meanwhile, there exist 3 6c-2e π bonds on the top, 3 5c-2e π bonds at the bottom, and 6 6c-2e π bonds around the waist over the σ skeleton. All the 118 valence electrons in C_3 Ca@B_{39}^+ (**1**) are thus delocalized in either multicenter σ or π bonds, forming an effective σ plus π double delocalization, which compensates for the electron deficiency of the boron cage. The 12 delocalized π bonds over the C_3 B_{39}^- cage may back-donate partial electron(s) to the empty Ca 3d atomic orbitals sprouting from inside, as reflected in the Ca electron configurations discussed above. The σ plus π double delocalization bonding pattern of C_3 Ca@B_{39}^+ (**1**) is actually the same as that of the bare C_3 B_{39}^-.[24] As shown in Fig. 3b, C_2 Ca@B_{39}^+ (**2**) also has the same bonding interaction as C_2 B_{39}^-.[24] Thus, as isovalent systems, C_3/C_2 Ca^{2+}@B_{39}^- (**1/2**) inherit both the axial chirality and bonding pattern of their C_3/C_2 B_{39}^- parents.

It is known that both C_3 B_{39}^- and C_2 B_{39}^- are dynamically stable at 200 K and fluctuate between low-lying structures above 300 K (*i.e.* above 300 K, C_3 B_{39}^- and C_2 B_{39}^- clusters "hop" between different cage-like structures in concerted mechanisms with low energy barriers; such structural transformations involve synergistic bond breakage and formation).[24] Extensive MD simulations (Fig. S2, ESI†) indicate that, when incorporated with a Ca atom inside, both C_3 Ca@B_{39}^+ (**1**) and C_2 Ca@B_{39}^+ (**2**) remain dynamically stable at 200 K, with the average root-mean-square-deviation (RMSD) of 0.07 and 0.07 Å and maximum bond length deviation (MAXD) of 0.28 and 0.27 Å, respectively. At 300 K, C_2 Ca@B_{39}^+ (**2**) maintains its structural integrity with RMXD = 0.08 Å and MAXD = 0.31 Å, while C_3 Ca@B_{39}^+ (**1**) starts to "hop" between C_3 (**1**), C_1 (**3**), and C_2 (**2**) configurations in concerted mechanisms with RMXD = 0.19 Å and MAXD = 0.86 Å. Further MD simulations show that both C_3 Ca@B_{39}^+ (**1**) and C_2 Ca@B_{39}^+ (**2**) fluctuate structurally between low-lying structures at 400 K (Fig. S2, ESI†), similar to C_3/C_2 B_{39}^-.[24] Overall, C_3/C_2 Ca@B_{39}^+ behave similar to C_3/C_2 B_{39}^- in molecular dynamics.

The combination of infrared photodissociation (IR-PD) spectroscopy and first-principles calculations has proven to be an effective approach in the characterization of novel cluster monocations.[43,44] We calculate here the vibrational frequencies and simulate the IR spectra of C_3/C_2 $Ca@B_{39}^+$ (**1**/**2**), as shown in Fig. 4a, and compared with those of C_3/C_2 B_{39}^- at DFT-PBE0. C_3 $Ca@B_{39}^+$ (**1**) appears to exhibit similar IR features with C_3 B_{39}^-, with the three strongest IR peaks at 1233 cm^{-1} (e), 1261 cm^{-1} (a), and 1310 cm^{-1} (e) in the latter well remained in the former (Fig. 4a). All other IR active vibrations are very weak. The IR vibrations associated with the Ca centre appear to lie below 230 cm^{-1}. The simulated Raman spectrum of C_3 $Ca@B_{39}^+$ is also similar to that of C_3 B_{39}^- (Fig. 4b). As expected, both the predicted IR and Raman spectra of C_2 $Ca@B_{39}^+$ (**2**) are similar with those of C_2 B_{39}^- (Fig. 4).

In conclusion, we have presented at first-principles level the viability of the first axially chiral metalloborospherenes C_3/C_2 $Ca@B_{39}^+$ (**1**/**2**), utilizing the experimentally known C_3/C_2 B_{39}^- as molecular devices. Bonding analyses reveal the universal σ plus π double delocalization of these $Ca@B_{39}^+$ complexes. Their IR and Raman spectra are predicted to be similar with those of their C_3/C_2 B_{39}^- parents. The axially chiral metalloborospherenes predicted in this work invite further theoretical and experimental investigations towards the formation of chiral borospherene-based nanomaterials.

Acknowledgements

This work was jointly supported by the National Natural Science Foundation of China (21243004), the Shanxi International Cooperation project (2013081018), and the State Key Laboratory of Quantum Optics and Quantum Optics Devices (KF201402). H.J.Z. gratefully acknowledges the start-up fund from Shanxi University.

Notes and references

1 J. R. Heath, S. C. O'Brien, Q. Zhang, Y. Liu, R. F. Curl, H. W. Kroto, F. K. Tittel and R. E. Smalley, *J. Am. Chem. Soc.*, 1985, **107**, 7779–7780.
2 Z. Wan, J. F. Christian and S. L. Anderson, *Phys. Rev. Lett.*, 1992, **69**, 1352–1355.
3 P. Weis, R. D. Beck, G. Bräuchle and M. M. Kappes, *J. Chem. Phys.*, 1994, **100**, 5684–5695.
4 Y. Kubozono, H. Maeda, Y. Takabayashi, K. Hiraoka, T. Nakai, S. Kashino, S. Emura, S. Ukita and T. Sogabe, *J. Am. Chem. Soc.*, 1996, **118**, 6998–6999.
5 L. S. Wang, J. M. Alford, Y. Chai, M. Diener, J. Zhang, S. M. McClure, T. Guo, G. E. Scuseria and R. E. Smalley, *Chem. Phys. Lett.*, 1993, **207**, 354–359.
6 M. Saunders, R. J. Cross, H. A. Jiménez-Vázquez, R. Shimshi and A. Khong, *Science*, 1996, **271**, 1693–1697.
7 T. A. Murphy, T. Pawlik, A. Weidinger, M. Höhne, R. Alcala and J. M. Spaeth, *Phys. Rev. Lett.*, 1996, **77**, 1075–1078.
8 J. Lu, X. W. Zhang and X. G. Zhao, *Chem. Phys. Lett.*, 1999, **312**, 85–90.
9 M. Waiblinger, K. Lips, W. Harneit, A. Weidinger, E. Dietel and A. Hirsch, *Phys. Rev. B: Condens. Matter Mater. Phys.*, 2001, **63**, 045421.
10 (*a*) T. Okazaki, Y. Lian, Z. Gu, K. Suenaga and H. Shinohara, *Chem. Phys. Lett.*, 2000, **320**, 435–440; (*b*) J. X. Xu, X. Lu, X. H. Zhou, X. R. He, Z. J. Shi and Z. N. Gu, *Chem. Mater.*, 2004, **16**, 2959–2964; (*c*) J. X. Xu, M. X. Li, Z. J. Shi and Z. N Gu, *Chem. – Eur. J.*, 2006, **12**, 562–567; (*d*) Y. Zhang, J. X. Xu, C. Hao, Z. J. Shi and Z. N. Gu, *Carbon*, 2006, **44**, 475–479.
11 H. J. Zhai, A. N. Alexandrova, K. A. Birch, A. I. Boldyrev and L. S. Wang, *Angew. Chem., Int. Ed.*, 2003, **42**, 6004–6008.
12 H. J. Zhai, B. Kiran, J. Li and L. S. Wang, *Nat. Mater.*, 2003, **2**, 827–833.
13 B. Kiran, S. Bulusu, H. J. Zhai, S. Yoo, X. C. Zeng and L. S. Wang, *Proc. Natl. Acad. Sci. U. S. A.*, 2005, **102**, 961–964.
14 W. Huang, A. P. Sergeeva, H. J. Zhai, B. B. Averkiev, L. S. Wang and A. I. Boldyrev, *Nat. Chem.*, 2010, **2**, 202–206.
15 E. Oger, N. R. M. Crawford, R. Kelting, P. Weis, M. M. Kappes and R. Hlrichs, *Angew. Chem., Int. Ed.*, 2007, **46**, 8503–8506.
16 W. L. Li, Y. F. Zhao, H. S. Hu, J. Li and L. S. Wang, *Angew. Chem., Int. Ed.*, 2014, **53**, 5540–5545.
17 W. L. Li, Q. Chen, W. J. Tian, H. Bai, Y. F. Zhao, H. S. Hu, J. Li, H. J. Zhai, S. D. Li and L. S. Wang, *J. Am. Chem. Soc.*, 2014, **136**, 12257–12260.
18 Z. A. Piazza, H. S. Hu, W. L. Li, Y. F. Zhao, J. Li and L. S. Wang, *Nat. Commun.*, 2014, **5**, 3113.
19 (*a*) A. N. Alexandrova, A. I. Boldyrev, H. J. Zhai and L. S. Wang, *Coord. Chem. Rev.*, 2006, **250**, 2811–2866; (*b*) C. Romanescu, T. R. Galeev, W. L. Li, A. I. Boldyrev and L. S. Wang, *Acc. Chem. Res.*, 2013, **46**, 350–358; (*c*) A. P. Sergeeva, I. A. Popov, Z. A. Piazza, W. L. Li, C. Romanescu, L. S. Wang and A. I. Boldyrev, *Acc. Chem. Res.*, 2014, **47**, 1349–1358.
20 N. G. Szwacki, A. Sadrzadeh and B. I. Yakobson, *Phys. Rev. Lett.*, 2007, **98**, 166804.
21 F. Y. Li, P. Jin, D. E. Jiang, L. Wang, S. B. Zhang, J. J. Zhao and Z. F. Chen, *J. Chem. Phys.*, 2012, **136**, 074302.
22 S. De, A. Willand, M. Amsler, P. Pochet, L. Genovese and S. Goedecker, *Phys. Rev. Lett.*, 2011, **106**, 225502.
23 H. J. Zhai, Y. F. Zhao, W. L. Li, Q. Chen, H. Bai, H. S. Hu, Z. A. Piazza, W. J. Tian, H. G. Lu, Y. B. Wu, Y. W. Mu, G. F. Wei, Z. P. Liu, J. Li, S. D. Li and L. S. Wang, *Nat. Chem.*, 2014, **6**, 727–731.
24 Q. Chen, W. L. Li, Y. F. Zhao, S. Y. Zhang, H. S. Hu, H. Bai, H. R. Li, W. J. Tian, H. G. Lu, H. J. Zhai, S. D. Li, J. Li and L. S. Wang, *ACS Nano*, 2015, **9**, 754–760.
25 Q. Chen, S. Y. Zhang, H. Bai, W. J. Tian, T. Gao, H. R. Li, C. Q. Miao, Y. W. Mu, H. G. Lu, H. J. Zhai and S. D. Li, *Angew. Chem., Int. Ed.*, 2015, **54**, 8160–8164.
26 H. Bai, Q. Chen, H. J. Zhai and S. D. Li, *Angew. Chem., Int. Ed.*, 2014, **54**, 941–945.
27 R. X. He and X. C. Zeng, *Chem. Commun.*, 2015, **51**, 3185–3188.
28 P. Schwerdtfeger, L. N. Wirz and J. Avery, *Wiley Interdiscip. Rev.: Comput. Mol. Sci.*, 2015, **5**, 96–145.
29 P. Jin, Q. H. Hou, C. C. Tang and Z. F. Chen, *Theor. Chem. Acc.*, 2015, **134**, 13–22.

30 S. Goedecker, W. Hellmann and T. Lenosky, *Phys. Rev. Lett.*, 2005, **95**, 055501.
31 S. Goedecker, *J. Chem. Phys.*, 2004, **120**, 9911–9917.
32 C. Adamo and V. Barone, *J. Chem. Phys.*, 1999, **110**, 6158–6170.
33 T. Yanai, D. P. Tew and N. C. Handy, *Chem. Phys. Lett.*, 2004, **393**, 51–57.
34 R. Krishnan, J. S. Binkley, R. Seeger and J. A. Pople, *J. Chem. Phys.*, 1980, **72**, 650–654.
35 M. J. Frisch, G. W. Trucks, H. B. Schlegel, G. E. Scuseria, M. A. Robb, J. R. Cheeseman, G. Scalmani, V. Barone, B. Mennucci and G. A. Petersson, *et al.*, *Gaussian 09, Revision B.01*, Gaussian Inc., Wallingford, CT, 2010.
36 J. Čížek, *Adv. Chem. Phys.*, 1969, **14**, 35–89.
37 G. D. Purvis III and R. J. Bartlett, *J. Chem. Phys.*, 1982, **76**, 1910–1918.
38 K. Raghavachari, G. W. Trucks, J. A. Pople and M. Head-Gordon, *Chem. Phys. Lett.*, 1989, **157**, 479–483.
39 H. J. Werner, P. J. Knowles, G. Knizia, F. R. Manby, M. Schütz, P. Celani, T. Korona, R. Lindh, A. Mitrushenkov and G. Rauhut, *et al.*, MOLPRO, version 2012.1.
40 J. V. Vondele, M. Krack, F. Mohamed, M. Parrinello, T. Chassaing and J. Hutter, *Comput. Phys. Commun.*, 2005, **167**, 103–128.
41 D. Yu. Zubarev and A. I. Boldyrev, *Phys. Chem. Chem. Phys.*, 2008, **10**, 5207–5217.
42 G. L. Gutsev and A. I. Boldyrev, *Chem. Phys.*, 1981, **56**, 277–283.
43 G. J. Wang, J. M. Cui, C. X. Chi, X. J. Zhou, Z. H. Li, X. P. Xing and M. F. Zhou, *Chem. Sci.*, 2012, **3**, 3272–3279.
44 G. J. Wang, M. F. Zhou, J. T. Goettel, G. J. Schrobilgen, J. Su, J. Li, T. Schlöder and S. Riedel, *Nature*, 2014, **514**, 475–477.

